



HAL
open science

Spin excitations in the antiferromagnet NaNiO_2

Sophie de Brion, Céline Darie, M. Hopzapfel, D. Talbayev, L. Mihaly, F. Simon, A. Janossy, G. Chouteau

► **To cite this version:**

Sophie de Brion, Céline Darie, M. Hopzapfel, D. Talbayev, L. Mihaly, et al.. Spin excitations in the antiferromagnet NaNiO_2 . *Physical Review B: Condensed Matter and Materials Physics (1998-2015)*, 2007, 75, pp.094402. 10.1103/PhysRevB.75.094402 . hal-00089093

HAL Id: hal-00089093

<https://hal.science/hal-00089093>

Submitted on 9 Aug 2006

HAL is a multi-disciplinary open access archive for the deposit and dissemination of scientific research documents, whether they are published or not. The documents may come from teaching and research institutions in France or abroad, or from public or private research centers.

L'archive ouverte pluridisciplinaire **HAL**, est destinée au dépôt et à la diffusion de documents scientifiques de niveau recherche, publiés ou non, émanant des établissements d'enseignement et de recherche français ou étrangers, des laboratoires publics ou privés.

Spin excitations in the antiferromagnet NaNiO_2

S. de Brion,¹ C. Darie,² M. Holzapfel,^{1,3} D. Talbayev,⁴ L. Mihály,^{4,5} F. Simon,⁶ A. Jánossy,⁶ and G. Chouteau¹

¹*Grenoble High Magnetic Field Laboratory, CNRS, BP 166, 38042 Grenoble, France*

²*Laboratoire de Cristallographie, CNRS, BP 166, 38042 Grenoble, France*

³*present address: Paul-Scherrer-Institut CH-5232 Villigen PSI, Switzerland*

⁴*Department of Physics, Stony Brook University, NY 11794-3800, USA*

⁵*Electron Transport Research Group of the Hungarian Academy of Science and Department of Physics, Budapest University of Technology and Economics, 1111 Budapest, Hungary*

⁶*Budapest University of Technology and Economics, Institute of Physics and Solids in Magnetic Fields Research Group of the Hungarian Academy of Sciences, P. O. Box 91, H-1521 Budapest, Hungary*

(Dated: August 10, 2006)

In NaNiO_2 , Ni^{3+} ions form a quasi two dimensional triangular lattice of $S = 1/2$ spins. The magnetic order observed below 20K has been described as an A type antiferromagnet with ferromagnetic layers weakly coupled antiferromagnetically. We studied the magnetic excitations with the electron spin resonance for frequencies 1-20 cm^{-1} , in magnetic fields up to 14 T. The bulk of the results are interpreted in terms of a phenomenological model involving bi-axial anisotropy for the spins: a strong easy-plane term, and a weaker anisotropy within the plane. The direction of the easy plane is constrained by the collective Jahn-Teller distortion occurring in this material at 480 K.

PACS numbers: 71.27+a, 75.30.Et, 71.70-d, 61.10.Nz, 75.40.Cx

I. INTRODUCTION

A two-dimensional triangular network of magnetic ions interacting via an antiferromagnetic interaction is a well known geometrically frustrated system where unconventional magnetic properties are expected [1]. Usually, a long range magnetic order occurs at low enough temperature. For instance, in XCl_2 with $\text{X}=\text{Cr}, \text{Br}$, or in ACrO_2 with $\text{A}=\text{Li}, \text{Ag}, \text{Cu}$, or CsCuCl_3 the magnetic order is based on a 120° spin structure on the triangles. All these compounds have an easy plane or easy axis anisotropy together with Heisenberg type antiferromagnetic interactions. In other compounds, no magnetic order was detected so far (NaCrO_2 , KCrO_2 , NaTiO_2 , LiNiO_2). The possibility of the orbital order competing with the spin order makes LiNiO_2 particularly interesting. In this compounds the Ni^{3+} ions have a spin $S = 1/2$ and the orbital occupation is doubly degenerate: the e_g orbitals, $|3z^2 - r^2\rangle$ and $|x^2 - y^2\rangle$, have the same energy unless the oxygen octahedron around the magnetic ion becomes elongated or compressed due to the Jahn-Teller effect.

Surprisingly, no orbital order has been observed in LiNiO_2 . The absence of both orbital and magnetic order in this compound has been the subject of intense debate lately, both experimentally [2] and theoretically [3]. In particular, there is still a controversy on what are the relevant magnetic interactions within the triangular planes and to what extent this compound is magnetically frustrated. The comparison with the isomorphous NaNiO_2 is aimed at elucidating this unconventional behavior. In NaNiO_2 a ferro-distortive orbital order (a collective Jahn-Teller distortion) is observed below 480 K [4] and a long range antiferromagnetic order appears below 20 K [5]. This magnetic order was first described as an A type

antiferromagnet with ferromagnetic planes coupled antiferromagnetically [5][6]. The magnetic superlattice has indeed been observed recently in neutron diffraction measurements [7]. However, the description of the magnetic system with just two magnetic interactions (an antiferromagnetic J_{AF} between subsequent NiO planes and a ferromagnetic J_F within the planes) fails to describe the whole magnetic behavior, in particular the presence of three characteristic fields observed in the magnetization curve [9]. The direction of the spins measured by neutron diffraction is also unusual: they point toward the center of one of the triangles in the oxygen octahedron surrounding each Ni ion, at 100° from the Ni plane [7]. Moreover, a recent inelastic neutron study [8] has shown that a gap of $\simeq 0.7$ meV is present in the spin excitation spectrum.

We have performed Electron Spin Resonance measurements in magnetic fields up to 14 T on powder samples of NaNiO_2 . We adopted and extended the model used to describe the magnon spectrum [8]. We find that the low field behavior of the system is characteristic of an "easy-plane" magnet, with a small anisotropy within the plane. The spin-flop transition is assigned to this latter anisotropy. At high fields all spins are aligned parallel and the saturation effects dominate the behavior. Although the model described here is generally successful, we also observed a spin resonance mode that remains unexplained. The possible implications for the magnetic interactions in LiNiO_2 are discussed.

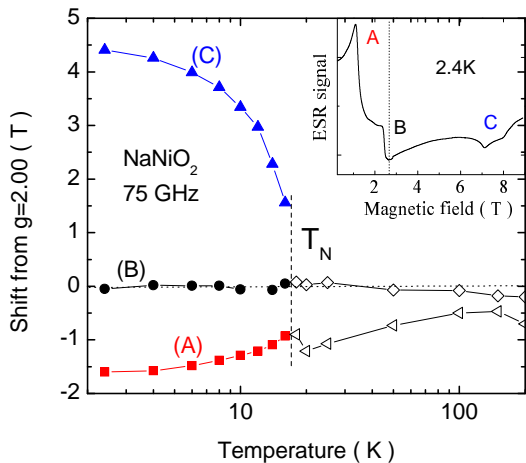


FIG. 1: Shift of the resonance lines position from the paramagnetic line at 75 GHz as a function of temperature. Insert: typical ESR spectrum as a function of magnetic field recorded at 2.4 K. The dotted line corresponds to the paramagnetic line at $g=2$.

II. EXPERIMENTS

The NaNiO_2 powdered sample was obtained following the procedure described elsewhere [4]. The monoclinic $C2/m$ crystal structure was checked by X-ray powder diffraction. The system is quasi two-dimensional: The Ni-Ni interplane distance is large, 5.568 Å. Below the Jahn-Teller transition at 480 K the Ni^{3+} ions are arranged in a slightly distorted triangular network, with one short length and two longer ones (at room temperature, the Ni-Ni distances are 2.84 Å and 3.01 Å respectively compared to 2.96 Å at 565 K) [4]. Also, the oxygen octahedra surrounding the nickel ions are elongated. Such a distortion favors the $|3z^2 - r^2\rangle$ orbitals. Indeed, the ESR spectra at 200K have the anisotropic shape typical of the $|3z^2 - r^2\rangle$ orbitals, with $g^{\parallel} = 2.03$ and $g^{\perp} = 2.28$ for fields parallel and perpendicular to z , respectively [4].

The magnetic behavior of our NaNiO_2 sample was the same as the one reported previously [9]. The magnetic susceptibility exhibits a Curie-Weiss behavior above 100 K. The Curie-Weiss temperature of $T_{\text{CW}}=36$ K reflects the predominance of ferromagnetic interactions. This is a noticeable difference compared to frustrated triangular compounds such as LiCrO_2 . The effective magnetic moment ($1.85 \mu_B$) is in agreement with the $|3z^2 - r^2\rangle$ orbital configuration for the e_g electron in the low spin state of Ni^{3+} (spin $S=1/2$, average gyromagnetic factor $g_{av} = 2.14$). The Néel temperature, observed as a peak in the susceptibility, is $T_N=20$ K. The magnetization curve in the ordered phase at 4 K presents two kinks at $H_{C0}=1.8$ T, $H_{C1}=8$ T, previously assigned to spin flop transitions, and the magnetization is fully saturated at $H_{\text{sat}}=13$ T [9].

The Electron Spin Resonance measurements (ESR)

were performed using two different techniques. Classical high frequency, high magnetic field ESR was used at fixed frequencies using Gunn diode oscillators and multipliers at 35, 75, 150 and 225 GHz, combined with a 9 T magnet at the Budapest University of Technology and Economics. Previous measurements at the Grenoble High Magnetic Field laboratory have been described in Ref. 5.

Other measurements were performed by a novel method [10, 11]. We used the far infrared facilities of the National Synchrotron Light Source in Brookhaven National Laboratory, at the U12 IR beamline, including a 14 T superconducting magnet (Oxford Instruments), and a Fourier Transform Infrared Spectrometer (Sciencetech, SPS 200). We will present results obtained in the frequency range $3 \text{ cm}^{-1} - 20 \text{ cm}^{-1}$ (90 GHz - 600 GHz) at 4 K. The powdered sample was in a disk-shaped teflon container of 5 mm diameter and 1 mm thickness, in the center of the magnet. Light pipes were used to guide the infrared light from spectrometer to the sample, and the transmitted light was detected with a bolometer operating at 1.2K temperature. The light propagated parallel to the static magnetic field. Spectra were recorded at fixed fields. The frequency resolution was selected at 0.2 cm^{-1} , much less than the width of the resonance lines. The upper frequency cut-off was adjusted to about 20 cm^{-1} with a Fluorogold filter of appropriate thickness. The lower cut-off was limited by the incident spectrum and the spectrometer performance. The signal to noise ratio was good down to 3 cm^{-1} , but there were strong minima in the incident light intensity around 3.7 and 4.6 cm^{-1} . We eliminated the experimental points at these minima without losing the data around them, obtaining reliable signal down to 3 cm^{-1} . After averaging over several spectra (typically between two and four) and smoothing, the absorption spectrum at a given field was divided by a reference spectrum recorded at zero magnetic field, following the same procedure as described in Ref. [11].

III. RESULTS

First, we present the ESR results obtained with the classical ESR technique. A typical spectrum (the derivative of the absorption signal), recorded at 2.4 K at 75 GHz in the antiferromagnetic phase, has three resonance features (Fig. 1). The lines labeled (A), (B), and (C) are shifted from the paramagnetic $g = 2$ line differently and they exhibit different temperature dependencies. Mode (A) has been already studied in [5] and was related to the spin flop field at 1.8 T. Mode (B) remains close to the paramagnetic line. Mode (C) consists of two close resonances which broaden with temperature and are hardly resolved above 6 K. Therefore only the first, larger intensity, resonance is plotted for the temperature dependence of mode (C). Below the phase transition temperature T_N , this mode behaves as the order parameter.

The paramagnetic line splitting at 200 K (empty symbols in Fig. 1) is in agreement with the line splitting studied in detail at several frequencies by Chappel *et al.* [4]. There is also an agreement in the temperature dependence of the splitting. We will discuss the paramagnetic state in a separate publication [15].

The measurements were done on powder samples, and therefore the large line broadening seen in Fig. 1 is not surprising. For any given crystallite in the sample, the line position depends on the relative direction of external field and the crystallographic axes. Relatively sharp features appear in the spectrum because in the powder sample certain resonance frequencies (*e.g.* the highest and the lowest possible values) acquire large statistical weight. This effect is well known from the powder samples with significant g -factor anisotropy.

It is also important to notice that the presence of three lines in the spectrum at finite field does not necessarily mean that the microscopic Hamiltonian of the system has three modes, for the same reasons as above. On the other hand, the number of modes seen at zero external field (where all crystallites are equivalent) are directly relevant to the Hamiltonian, as we will discuss later.

The low temperature ESR was further explored by far infrared spectroscopic methods. The advantage of detecting ESR by far-IR spectroscopy is that one can readily map the power absorption over the full range of magnetic fields and frequencies. The measurement does not rely on sweeping the magnetic field; this becomes especially important when one tries to discern features at zero field, or compare ESR to inelastic neutron scattering done in zero field.

Typical absorption spectra at 0 T and 14 T recorded at 4 K are given in Fig. 2. The sharp peaks in the spectra are "instrumental": either due to interference features in the synchrotron source, or generated by the multiple reflections in the sample, or in the spectrometer itself. Nevertheless, the absorption due to spins is clearly visible with features around 6 cm^{-1} (labeled (1)), 9 cm^{-1} (labeled (2)) and $11\text{-}18 \text{ cm}^{-1}$ (labeled (M)).

The key to these measurements is taking the ratio of two data sets at different fields, eliminating the features in the raw spectrum of the incident light, and leaving field dependent part of the absorption. We have chosen always the same reference: the spectrum at zero field, so that the relative transmission I_r is related to the sample absorption $I_{\text{spin}}(H)$:

$$I_r(H) = I_N(H)/I_{\text{spin}}(0). \quad (1)$$

The relative transmission for $H=14 \text{ T}$ is plotted in the bottom part of fig. 2. The data below 3 cm^{-1} are not reliable. A smoothing procedure using a FT filter has been used to improve the signal to noise ratio. It is responsible for the weak oscillations with the 2 cm^{-1} periodicity. The relative transmission data for several magnetic fields are plotted in Fig. 3 for the frequency range 4 cm^{-1} - 20 cm^{-1} . An average over 3 to 4 data has been used. Below 10 cm^{-1} two broad peaks ((1) and (2)) lie above 1,

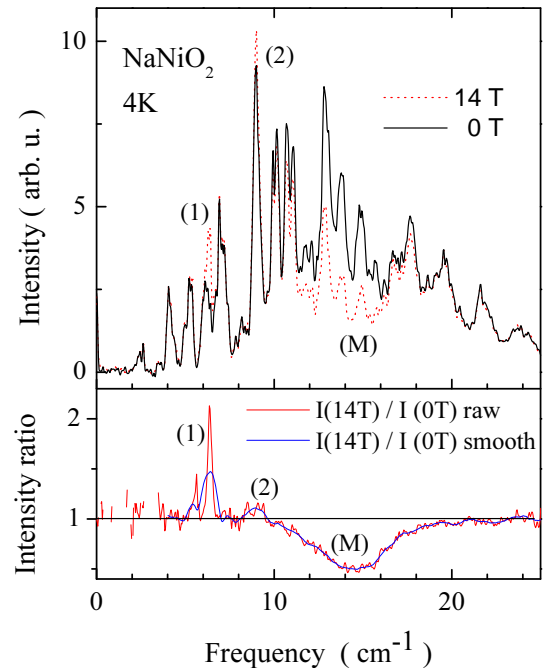


FIG. 2: upper part: Typical FT-ESR spectra recorded at 4 K, 0 T and 14 T. Lower part: Intensity ratio.

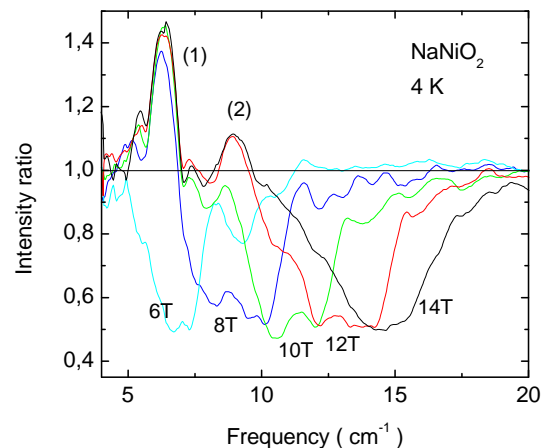


FIG. 3: FT-ESR Relative transmission $I_r(H)$ as a function of the electromagnetic wave frequency at different magnetic field values H .

indicating that the absorption $I_{\text{spin}}(0)$ presents two resonance modes. From all these relative transmission data, we can deduce the frequency dependence of $I_{\text{spin}}(0)$ and then $I_{\text{spin}}(H) = I_r(H) \times I_{\text{spin}}(0)$ for each magnetic field value.

All these results can be mapped on a frequency / magnetic field diagram (Fig. 4). The symbols correspond to maxima in the derivative of the ESR absorption measured by field sweep at fixed frequencies, the colors are derived from the absorption $I_{\text{spin}}(H)$ measured at fixed fields. The main branch (M) is a broad signal, with frequency approximately proportional to the field, signifi-

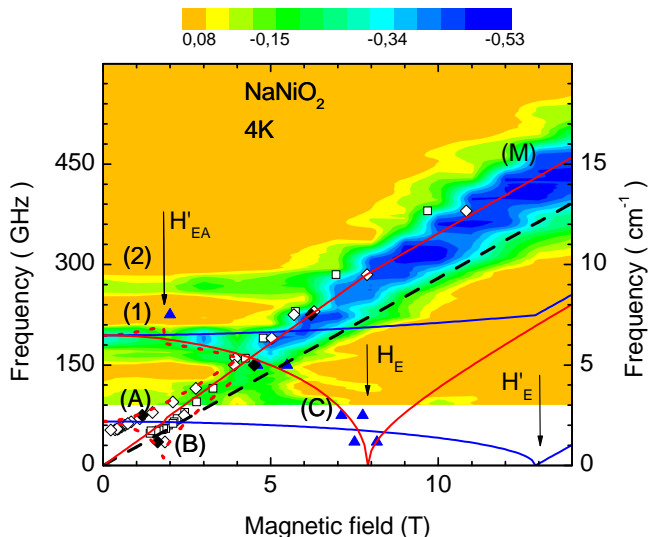


FIG. 4: Magnetic modes at 4 K in a frequency versus field map obtained from the resonance lines positions in conventional ESR (closed symbols: this work; open symbols: from [5]) and the transmission I_{spin} in FT-ESR (the color scale on the top refers to the intensity of the signal, as shown in Fig. 3). The dash black line corresponds to the paramagnetic resonance at $g = 2$. The blue and red continuous lines represent the calculated frequencies ω^{\parallel} and ω^{\perp} corresponding to fields parallel and perpendicular to the hard axis, respectively. The red dotted lines, ω^{int} , are for fields along the intermediate axis (see appendix B).

cantly above the $g = 2$ line. Mode (A) and (B) are related to the spin-flop transition observed at 1.8 T in the magnetization curve [6]. Mode (A) has been discussed previously [5] in terms of an easy axis antiferromagnet model [5]. The field dependence of this mode is typical of crystallites in the powder where the static field is perpendicular to the easy axis. When the magnetic field is along the easy axis, a spin-flop transition occurs at 1.8 T. Crystallites oriented in this direction contribute to Mode (B).

Modes (1) and (2) are seen mostly in the far-IR measurements, with supporting evidence from a field sweep at 225 GHz. These modes have very little field dependence. The corresponding zero field gaps are 6.5 and 9.0 cm^{-1} , respectively (0.85 and 1.1 meV). Mode (1) at 0.85 meV is close to the dispersionless magnon mode observed at 0.7 meV in inelastic neutron scattering measurements [8]. Mode (1) crosses the main branch, and it appears again at low frequencies, labelled as mode (C), also seen in Fig. 1. Apparently, this mode softens to zero frequency around 8 T.

Further information can be deduced from a quantitative analysis of the IR absorption data. We will assume that the absorption $I_{\text{spin}}(H)$ can be approximately related to the dissipative spin susceptibility χ'' :

$$\ln I_{\text{spin}}(H) = \frac{-4\pi nd}{c} \chi''(H) \quad (2)$$

where c is the vacuum speed of light, n the refraction index, d is thickness of the sample and ω the light frequency. The absorption peaks $\chi''(H)$ are well fitted with a Gaussian lineshape (see insert in Fig. 5b). The corresponding resonance frequency, linewidth and total area are plotted as a function of the applied magnetic field (Fig. 5a, b, and c respectively). Note that the line positions are unchanged whether one looks at $I_{\text{spin}}(H)$ or $\chi''(H)$. The line position and line width confirm that the resonance associated with the main branch (M) is nearly paramagnetic with $g \approx 2.2$. Its linewidth is in accordance with the linewidth calculated from the g anisotropy at 200 K. However the anisotropic line shape observed at 200 K is no longer present here, presumably due to additional lifetime broadening. The branches (1) and (2) are clearly identified at 6.5 cm^{-1} and 9 cm^{-1} with no field dependence until they both merge into the main branch (M).

The area under the absorption peak is related to the ESR susceptibility through the Kramers-Kronig relation:

$$\chi(H, 0) \propto \int \frac{\chi''(H, \omega)}{\omega} d\omega \simeq \frac{1}{\omega_0} \int \chi''(H, \omega) d\omega \quad (3)$$

where ω_0 is the peak position. For the main branch (M), ω_0 is proportional to the static field H . Then the peak area $\int \chi''(H, \omega) d\omega$ scales with the static magnetization. This is indeed observed in Fig. 5c. The saturation of the total intensity above 9 T is in accordance with the saturation of the static magnetization observed in this material [9]. For branches (1) and (2), ω_0 is constant. Then the peak area is proportional to the static susceptibility $\chi(H, 0)$. For both modes, it is constant with the field, as is expected away from spin-flop field transitions. One can also see that mode (2) has a weaker susceptibility than mode (1). Note that this susceptibility measured on a powder sample includes the statistical weight associated with the crystallites in the powder which are oriented correctly as regards the magnetic field direction for each resonance mode.

IV. DISCUSSION

Several models have been proposed to describe the magnetic properties in this material. The first one assumes a uniaxial easy axis antiferromagnet, proposed by Bongers *et al.* [6] to account for the spin-flop transition at 1.8 T and then used in Ref. [5] for the ESR magnon branch at 53 GHz (branch (A) in Fig. 4). This model includes a strong ferromagnetic coupling in the Ni planes, a weaker antiferromagnetic coupling between the Ni planes and an even weaker anisotropy which aligns the spins in the easy axis direction. It was shown later that this model was incomplete in terms of explaining the magnetic properties, and an additional energy scale was required [9]. This conclusion was confirmed by recent neutron inelastic scattering measurements [8]. The

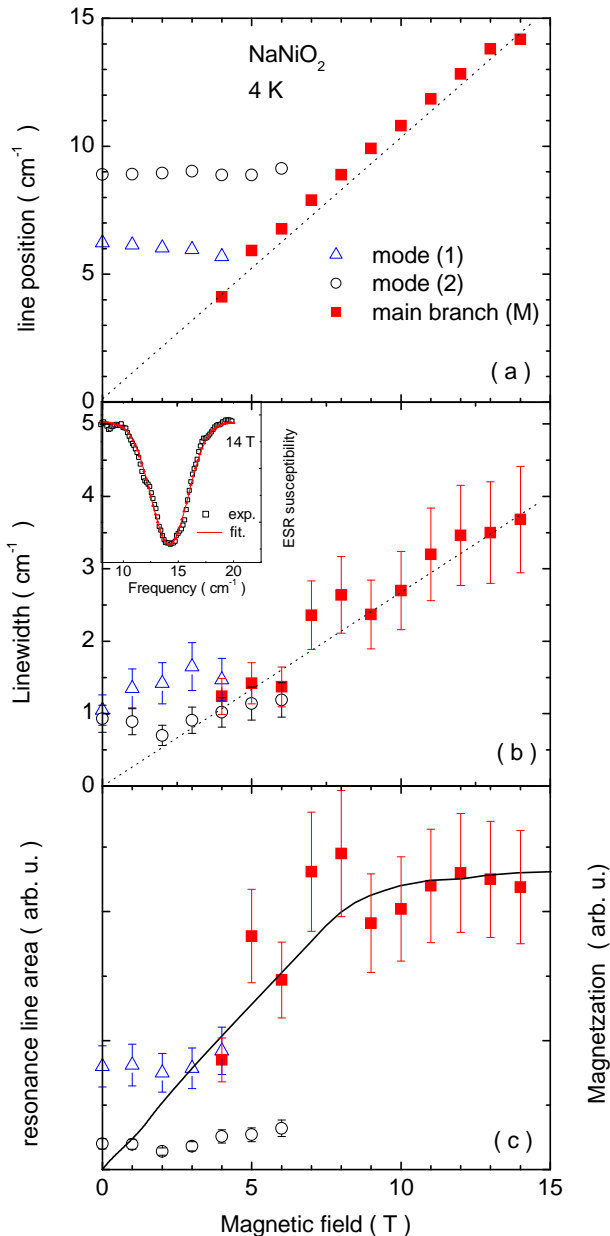


FIG. 5: Gaussian fit of FT-ESR susceptibility at 4 K: line position (a), line width (b) and line total area (c) together with the sample magnetization (continuous line) as a function of applied magnetic field. The dotted line in (a) corresponds to the paramagnetic line at $g=2.2$ and in (b) to a g anisotropy linewidth $\Delta g=0.26$. Insert: gaussian fit of the ESR susceptibility.

magnon spectrum was interpreted in terms of an easy plane AF model with the same ferromagnetic and antiferromagnetic couplings as in the previous model. The anisotropy was assigned to the ferromagnetic exchange coupling, and its magnitude was an order of magnitude larger than the weak anisotropy used in the evaluation of the ESR data.

These models were merged by assuming an anisotropy

tensor that has an easy axis within an easy plane, with a much larger energy needed for turning the spins out of the plane than within the plane. This simple approach accounts for most of the experimental observations, including a better description of the low field ESR data of Chappel et al.[5]. We start with the following anisotropic spin Hamiltonian:

$$\mathcal{H}_0 = \sum_{ab} \mathbf{S}_i \overleftrightarrow{\mathcal{J}}_{ab} \mathbf{S}_j + \sum_c \mathbf{S}_i \overleftrightarrow{\mathcal{J}}_c \mathbf{S}_j + g\mu_B \mathbf{S} \mathbf{H} \quad (4)$$

where \mathbf{H} is the magnetic field, \sum_{ab} is over nearest neighbor spins within the layers, and \sum_c is over nearest neighbor spins along the c directions. The exchange interactions are represented by tensors: $\overleftrightarrow{\mathcal{J}}_{ab}$ describes the ferromagnetic intraplane exchange, and $\overleftrightarrow{\mathcal{J}}_c$ is the interplane antiferromagnetic exchange. The intensity and the frequency of the spin resonance lines for a crystal positioned in arbitrary direction relative to the external field can be calculated from the Hamiltonian in two steps. First, the spin configuration is determined by minimizing the free energy; second the ESR frequencies are related to the small oscillations around the equilibrium configuration. There are two resonance modes for any given direction when the magnetic order is described by two sublattices. Occasionally (in zero field or field applied along high-symmetry directions) the two modes may be degenerate.

The powder spectrum is obtained by the average of the absorption of individual grains over all directions. In practice, the calculation of frequency and intensity for arbitrary field orientation is rather hard. Instead, the resonance frequency is calculated for the static field pointing in three principal directions. The six "principal frequencies" (three frequencies for each of the two modes) play a special role in the powder average, since some of them correspond to extremal values and the statistical weight factor for these frequencies will be high.

This process is similar to the determination of the \overleftrightarrow{g} tensor from the paramagnetic resonance of a powder sample with a g -factor anisotropy. Naturally, the orientation of the principal axes of the tensor relative to the crystallographic directions cannot be determined from measurements on a powder sample. Nevertheless, the \overleftrightarrow{g} -tensor components are routinely determined from powder measurements this way. It is often sufficient to look at the highest and lowest frequencies in the measured broad ESR line, and one can identify the highest and lowest tensor components.

There is an extensive literature on the anisotropy effects in antiferromagnets, starting with the early work of Keffer and Kittel [12] on the easy axis problem. The three axis case (easy, intermediate, hard) was treated by Nagamiya [13]. Here we base our analysis on this work and on a review by Turov [14]. The magnon spectrum is treated in the linear approximation, equivalent to a quasi-classical treatment and we focus on the ground state properties ($T=0$ K). The details of the calculation

are given in Appendix A and B. First, the Hamiltonian is transformed into:

$$\mathcal{H}_{MF}/N = \frac{A}{2}\mathbf{m}^2 + \frac{a}{2}m_z^2 + \frac{b}{2}l_z^2 + \frac{c}{2}m_x^2 + \frac{d}{2}l_x^2 - \mathbf{m}\mathbf{h}, \quad (5)$$

where \mathbf{m} and \mathbf{l} are the total magnetization and the antiferromagnetic order parameter, respectively. Parameter A describes an isotropic antiferromagnetic coupling, a and c describe the anisotropy of the total ferromagnetic moment. In the ideal antiferromagnetic state $\mathbf{m} = 0$, therefore these parameters have no influence on the free energy of the system in zero external magnetic field. On the other hand, parameters b and d act on the order parameter \mathbf{l} directly. Kittel treated the uniaxial model ($c = d = 0$) at low fields; easy plane and easy axis corresponds to $b > 0$ and $b < 0$, respectively. Nagamiya's biaxial model is obtained when $a = c = 0$. Turov discusses the uniaxial case for fields up to the saturation field [14].

We set $b > 0$ so that the zero field equilibrium magnetizations are in the plane perpendicular to z ; this will be the "easy plane". The anisotropy within the plane, represented here by coefficients c and d , is much smaller: $c, d \ll b$. (Notice that these choices do not follow from the symmetry arguments related to the lattice distortion, but they were forced by the experimental observations). Since c and d have similar effects on the spin resonance frequencies, and we can not determine them separately, we will assume that $d = 0$. This leaves us with four parameters to determine: A, a, b and c . For $c < 0$, x will be the easy direction, y will be the intermediate direction, and z remains the hard direction.

To facilitate the discussion, it is convenient to introduce the "effective fields" $H_E = A/M_0$, $H'_E = (A + a)/M_0$, and $H''_{EA} = \sqrt{Ac}/M_0$ where M_0 is the saturation magnetization (more effective fields follow in Appendix B). For applied field perpendicular to the hard axis the spin system saturates at H_E , when the external field overcomes the exchange field. For applied field parallel to the hard axis the saturation occurs at H'_E [14]. There is a spin-flop transition for field along the easy axis at $H = H''_{EA}$ [13].

The published susceptibility data, Fig. 4 of Ref. 9 can be used to find all but one of the parameters of the model. The first peak in the dM/dH curve at 1.8 T has been already identified as the spin-flop field H''_{EA} [5]. At around 8 T the dM/dH curve has a shoulder. We identify this as the onset of the saturation, and the corresponding field is H_E . Finally, the saturation is complete around 13T, corresponding H'_E . From these values we get $A = 8 T$, $a = 5 T$ and $c = -0.42 T$.

The parameter b determines the ESR frequency ω_2 at zero field. We selected $b = 6 T$ to match the zero field gap at 6.5 cm^{-1} (Mode (1) in Figures 4 and 5. This is quite close to the dispersionless magnon mode seen in neutron scattering ($0.7 \text{ meV} = 5.6 \text{ cm}^{-1}$) [8].

The principal frequencies are listed in Appendix B, and

the results are shown in Fig. 4. Considering that many of the parameters of the model were taken from other measurements, the agreement with the experiment is excellent. The calculated zero field resonance ω_1^{hard} is very close to the measured one at 53 GHz [5]. In fact, the low field behavior of our model (where the slope $d\omega/dH$ is zero for $H \rightarrow 0$) fits the lower branch in Fig. 8 of Ref. 5 better than the uniaxial easy axis model used in that work (where the $d\omega/dH = -\gamma$). Mode (1) is identified with ω_2 . As the field is increased, this mode is approximately independent of the field for any field direction. Therefore the powder signal remains narrow, and it is clearly visible in the fixed-field far-IR spectroscopy scans.

Field-independent modes, like the ω_2^{hard} and ω_2^{int} modes here, are very hard to detect in the field-sweep scan commonly used with the fixed-frequency methods. However, the spin-flop transition that occurs in the part of the sample where the field is close to the easy direction causes a jump in the frequency of ω_2^{easy} . This jump creates a measurable signal in the field-sweep scan [13]. In our case the 225 GHz fixed frequency ESR measurement was just in the right frequency range to catch this feature.

Above 5 T the powder average signal originating from ω_2 broadens and merges with other absorption. It can not be seen in the far-IR measurement, and only the (more sensitive) fixed frequency study picks it up as Mode (C). The upper extremum of all possible frequencies, ω_1^\perp , yields a strong signal. Although the g -factor was not adjusted ($g = 2$), the coefficient $\sqrt{1 + H_a/H_E}$ seen in Eq. 13 brings ω_1^\perp right into the middle of the experimental values of the main branch (M).

With the set of parameters $A=8 T$, $a=5 T$, $b=6 T$ and $c=-0.42 T$, we can deduce the coupling energies in the Hamiltonian described by Eq. 4. For the antiferromagnetic coupling we get $J_{AF}^z = A/3=3.58 \text{ K}$. The anisotropy of the ferromagnetic interaction is $J_F^z - J_F^y = (a + b)/3=4.93 \text{ K}$, comparable to the antiferromagnetic coupling. The anisotropy of the antiferromagnetic coupling is weak $J_{AF}^z - J_{AF}^y = (a - b)/3=0.45 \text{ K}$. The ferromagnetic coupling, deduced from the Curie-Weiss temperature, $J_F^z = -15 \text{ K}$, is the dominant interaction. This hierarchy of interactions was also deduced from inelastic neutron scattering by Lewis *et al.*[8] using a similar model.

The weak anisotropy within the easy plane can be assigned to the ferromagnetic or antiferromagnetic couplings or a combination of the two. The parameter c represents the sum of the two anisotropies: $2c/3 = (J_F^x - J_F^z) - (J_F^y - J_F^z) + (J_{AF}^x - J_{AF}^z) - (J_{AF}^y - J_{AF}^z) = -0.37 \text{ K}$. However, the measurements would be compatible with other combinations of these parameters (as long as the sum is fixed). For example all anisotropy may be in the ferromagnetic coupling $(J_F^x - J_F^z) - (J_F^y - J_F^z) = -0.37 \text{ K}$ and no anisotropy in the antiferromagnetic coupling, $(J_{AF}^x - J_{AF}^z) - (J_{AF}^y - J_{AF}^z) = 0$.

We tested the model with various other choice of parameters, partially disregarding the three characteris-

tic fields obtained from the susceptibility measurement. Decreasing a to zero fails to describe the flatness of mode (1). Negative values of a do not give good fits. The agreement with the data is still reasonably good. In the special case the uniaxial anisotropy of the antiferromagnetic interplane coupling, $J_{AF}^z - J_{AF}^y$, is exactly zero.

In spite of the general agreement between the model and the experiment, there are two features that are unexplained: the splitting of mode (C) at low temperature (Figure 1, insert) and the existence of mode (2).

The splitting of mode (C) is consistent with our model. This mode is detected when the field is perpendicular to the hard axis. Note that the calculations were done with $c = 0$, but in the presence of a finite c the saturation field may be slightly different for spins along the easy and intermediate axes. The magnetic field parameter $|c| = 0.42$ T is in the right range to explain the observed splitting.

The existence of mode (2) is entirely beyond the simple model presented here. The two-sublattice Hamiltonian yields two modes at zero field, and we have those two modes identified as mode (A) at 1.75 cm^{-1} (53 GHz) and mode (1) at 6.5 cm^{-1} . No room is left for mode (2) in this model.

V. CONCLUSION

We studied the field dependence of the ESR in NaNiO_2 and we interpreted the results in terms of a model involving anisotropic exchange interactions. The main interaction is ferromagnetic in the triangular NiO plane. It is an order of magnitude larger than the interplane antiferromagnetic coupling. The anisotropy in the ferromagnetic coupling is characterized by an uniaxial "easy plane" parameter of $a + b = 11$ T, and a much weaker easy axis parameter of $c = -0.42$ T.

One of the main results of our work is that the easy direction is only slightly better than the other directions perpendicular to the hard axis. This is in general agreement with the inelastic neutron scattering result, where the magnon spectrum was modeled with an easy plane spin Hamiltonian [8]. For the easy plane system one of the magnon modes has zero energy (in zero field and at zero wavenumber). The anisotropy within the easy plane pushes this magnon mode to a finite energy (1.8 $\text{cm}^{-1} = 0.2$ meV). This second magnon gap is small, and therefore it is not visible in the neutron scattering, but it is clearly seen in the ESR studies.

The principal axes of the anisotropy tensor were constrained by symmetry considerations (see appendix A), but cannot be determined uniquely. In order to reconcile our results with the magnetization measurements on a twinned crystal [6] and with the neutron diffraction results [7], where the spin orientation was measured, the easy direction (the x axis of the reference frame) was selected so that it makes a 100° angle to the ab plane (see Fig. 6). The hard axis was selected within the triangu-

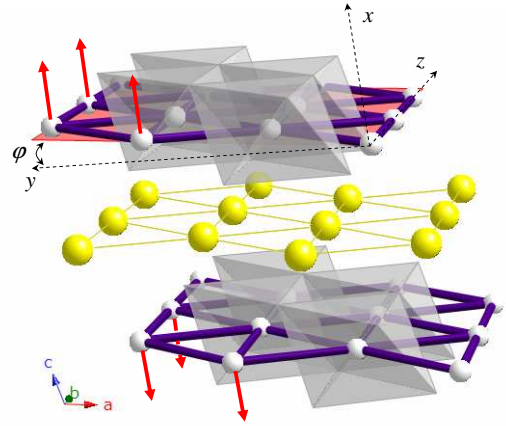


FIG. 6: The orientation of the hard axis z and the easy axis x relative to the triangular Ni layers. The ab plane is highlighted in the top layer. The z axis is parallel to the b direction in the crystal; the angle between the ab plane and the y axis is $\varphi \approx 10^\circ$. The spin directions are indicated by red arrows.

lar nickel plane, along the b direction of the crystal (Fig. 6). Alternatively, it may point in the y direction of the reference frame. The hard axis is probably related to spin-orbit effects on the ferromagnetic exchange. Indeed, the ratio $|(J_F^z - J_F^y)/J_F^y| = 0.33$ is comparable to the spin-orbit effect on the g tensor: $(g^\perp - g^\parallel)/g^\parallel = 0.10$. The choice of the easy axis involves an energy scale one order of magnitude smaller.

The existence of a third zero-field mode (mode 2) may point beyond the model used here: any two-sublattice model, that assumes that the magnitude of the sublattice magnetisations are fixed, yields at most two resonance modes in zero field. One can then think of quantum effects. They may cause some modes to shift from zero to finite frequencies [16], but do not change the number of modes. The comparison with other triangular magnets having antiferromagnetic coupling *within* the layers is intriguing: (including CsNiBr_3 , RbNiBr_3 , CsMnI_3 , CsMnBr_3 , CsCuCl_3 , RbCuCl_3 and $\text{RbFe}(\text{MoO}_4)_2$). There, typically three or six ESR modes [16, 17, 18] are observed. This is related to the umbrella-like spin order with, for a given triangle, each spin pointing at 120° from each other. Three sublattices are definitely present. This is not supposed to be the case in NaNiO_2 where there is strong support that the coupling within the triangular layers is ferromagnetic (the Curie-Weiss temperature is positive and the neutron diffraction patterns correspond to a A type antiferromagnet with ferromagnetically aligned spins in the layers [7]). However the sign of the interactions in the triangular planes has been the subject of intense debate in the isomorphic compound LiNiO_2 [2]. Even for NaNiO_2 a recent calculation by Vernay *et al* [3] proposes that one out of three interactions bond in the triangles are antiferromagnetic leading to antiferromagnetic chains, although this magnetic structure has not been observed experimentally. More

over, in the intermediate compound $\text{Li}_{0.3}\text{Na}_{0.7}\text{NiO}_2$ [9], which, on the orbital sector, behaves as LiNiO_2 and, on the spin sector, presents a long range antiferromagnetic order as in NaNiO_2 , we also observe the occurrence of three modes at zero field (around 0, 5.2 and 6.5 cm^{-1}); there the magnetic structure has not been solved yet. It is tempting to assign these similar behaviors to the presence of additional antiferromagnetic interactions. Further studies, preferably on single crystals, may solve this remaining puzzle in the $\text{NaNiO}_2/\text{LiNiO}_2$ layered triangular compounds.

VI. ACKNOWLEDGEMENT

We are indebted to G.L. Carr for valuable discussions and for developing the IR facilities at the NSLS, F. Mila, F. Vernay, C. Lacroix and M.D. Núñez-Regueiro for their theoretical inputs. S. de Brion acknowledges the Université Joseph Fourier for a CRTC program. The Budapest authors acknowledge the Hungarian State Grants (OTKA) TS049881, T60984 and F61733, and the MERG-CT-2005-022103 EU Project. F.S. acknowledges the Magyary program for support, L.M. acknowledges the Szent-Györgyi fellowship. The Grenoble High Magnetic Field Laboratory is "laboratoire Conventioennée à L'Université Joseph Fourier". Use of the National Synchrotron Light Source, Brookhaven National Laboratory, was supported by the U.S. Department of Energy, Office of Science, Office of Basic Energy Sciences, under contract No. DE-AC02-98CH10886.

VII. APPENDIX A: DERIVATION OF THE MEAN FIELD HAMILTONIAN AND SYMMETRIES

In the molecular field approximation the spins are assigned to two sublattices: Spins in the even layers are labeled by μ and spins in the odd layers are labeled by ν . \mathbf{S}_i and \mathbf{S}_j in the Hamiltonian are replaced with their average values, $\mathbf{S}_1 = 2/N \sum \mathbf{S}_\mu$ and $\mathbf{S}_2 = 2/N \sum \mathbf{S}_\nu$, where N is the total number of spins.

First, let us look at the term $\sum_{ab} \mathbf{S}_i \overleftrightarrow{\mathcal{J}}_{ab} \mathbf{S}_j$ in the Hamiltonian Eq. 4. All of the spins in this sum belong to the same sublattice, so the terms to add up will have the form of $\mathbf{S}_1 \overleftrightarrow{\mathcal{J}}_{ab} \mathbf{S}_1$ and $\mathbf{S}_2 \overleftrightarrow{\mathcal{J}}_{ab} \mathbf{S}_2$. For any given spin within a ferromagnetic layer, there are six neighbors, approximately positioned on the corners of a hexagon. Even though the exchange $\overleftrightarrow{\mathcal{J}}_{ab}$ with any one of this neighbors may be anisotropic, in the sum of the six terms most of

the anisotropy within the plane will be cancelled. In fact, as long as the exchange couplings can be represented by tensors, in an undistorted lattice the cancellation will be exact. The corresponding part of the Hamiltonian would be: $\sum_{ab} \mathbf{S}_i \overleftrightarrow{\mathcal{J}}_{ab} \mathbf{S}_j = (N/2)(1/2)6(\mathbf{S}_1 \overleftrightarrow{\mathcal{J}}_F \mathbf{S}_1 + \mathbf{S}_2 \overleftrightarrow{\mathcal{J}}_F \mathbf{S}_2)$, where the effective coupling $\overleftrightarrow{\mathcal{J}}_F$ is isotropic within the plane, the extra factor of 1/2 compensates for the double counting of each bond and the factor 6 reminds us that this exchange is an average over six bonds. Similar arguments can be used for the antiferromagnetic interlayer coupling to derive $\overleftrightarrow{\mathcal{J}}_{AF}$ from a sum over $\overleftrightarrow{\mathcal{J}}_c$'s. The proper reference frame for the new coupling tensors has the x direction perpendicular to the layers. The (equivalent) y and z directions are within the layers.

The anisotropy of the effective couplings $\overleftrightarrow{\mathcal{J}}_F$ and $\overleftrightarrow{\mathcal{J}}_{AF}$ is related to the distortion of the lattice. While above 480 K all nearest neighbor Ni-Ni bond lengths are equal [4], below the transition one side of the triangular lattice (along the b direction) is compressed, and two other sides are elongated. The $a-c$ plane remains a mirror plane, but the direction perpendicular to the layers is not a high symmetry direction anymore. (See Fig. 6.) Accordingly, the x direction will tilt relative to the direction perpendicular to the layers, as it acquires a non-zero component in the crystallographic a direction. At the same time the anisotropy axes within the plane become well defined. We will take the z axis parallel to the b crystallographic direction. The y axis will point slightly out of the plane, being perpendicular x and z . Notice that, except for permutations of the x, y, z labels, this is the only selection satisfying the broken crystal symmetries. The magnitude of the tilt of the x axis, and the amount of anisotropy, remain a free parameters. Similar arguments apply to the nearest neighbor antiferromagnetic coupling between the layers.

Spin resonance on a powder sample can be used to evaluate the anisotropy parameters of the resonance line. As we will see later, our system is described by a model with a dominant "easy plane" anisotropy, and a much weaker anisotropy within the plane. However, the orientation of the anisotropy axes relative to the crystal cannot be determined from a powder measurement. Neutron diffraction [7] and single crystal magnetization data [6] indicate that the easy axis makes an angle of approximately 100° to the NiO planes. We select this to coincide with the easy direction (the x axis of the reference frame). The hard axis may be either along y or z ; both choices agree with existing symmetries. We tentatively pick the z direction for the hard axis.

The mean field Hamiltonian becomes:

$$\begin{aligned} \mathcal{H}_{MF} = & \frac{3N}{2} [J_F^x(S_{1x}^2 + S_{2x}^2) + J_F^y(S_{1y}^2 + S_{2y}^2) + J_F^z(S_{1z}^2 + S_{2z}^2)] + \\ & + 3N (J_{AF}^x S_{1x} S_{2x} + J_{AF}^y S_{1y} S_{2y} + J_{AF}^z S_{1z} S_{2z}) + \frac{N}{2} g\mu_B (\mathbf{S}_1 + \mathbf{S}_2) \mathbf{H} \end{aligned} \quad (6)$$

The dimensionless sublattice magnetizations are defined as $\mathbf{m}_1 = \frac{1}{2}\mathbf{S}_1/S$ and $\mathbf{m}_2 = \frac{1}{2}\mathbf{S}_2/S$. When thermal and quantum fluctuations are neglected, the length of these vectors is fixed $|\mathbf{m}_1| = |\mathbf{m}_2| = 1/2$. Accordingly, we can express one of the sublattice magnetization components with the other two: $m_{1z}^2 = 1/4 - m_{1x}^2 - m_{1y}^2$ and $m_{2z}^2 = 1/4 - m_{2x}^2 - m_{2y}^2$. The Hamiltonian is:

$$\begin{aligned} \mathcal{H}_{MF} = & 12NS^2 [(J_F^x - J_F^z)(m_{1x}^2 + m_{2x}^2) + (J_F^y - J_F^z)(m_{1y}^2 + m_{2y}^2)] + \\ & + 6NS^2 (J_{AF}^x m_{1x} m_{2x} + J_{AF}^y m_{1y} m_{2y} + J_{AF}^z m_{1z} m_{2z}) + NSg\mu_B (\mathbf{m}_1 + \mathbf{m}_2) \mathbf{H} \end{aligned} \quad (7)$$

and we dropped a constant term proportional to J_F^z . In the absence of fluctuations the magnitude of the ferromagnetic coupling becomes irrelevant, only the anisotropy matters. Interestingly, the anisotropy term obtained here for the ferromagnetic coupling cannot be distinguished (within the molecular field approximation) from a microscopic "single ion" spin anisotropy. However, the physical origins are different: For spin 1/2 the microscopic single ion anisotropy can be shown to be exactly zero, whereas the same arguments do not apply here, where the anisotropy is due to the ferromagnetic exchange coupling.

The easy plane anisotropy around the z axis corresponds to $(J_F^x - J_F^z) \approx (J_F^y - J_F^z)$ (and similarly for the antiferromagnetic coupling). We can re-arrange the terms to better reflect this fact. For m_1 we get

$$\begin{aligned} & (J_F^x - J_F^z)m_{1x}^2 + (J_F^y - J_F^z)m_{1y}^2 = \\ & = 1/2[(J_F^x - J_F^z) + (J_F^y - J_F^z)](m_{1x}^2 + m_{1y}^2) + 1/2[(J_F^x - J_F^z) - (J_F^y - J_F^z)](m_{1x}^2 - m_{1y}^2) = \\ & = 1/2[(J_F^x - J_F^z) + (J_F^y - J_F^z)](1 - m_{1z}^2) + 1/2[(J_F^x - J_F^z) - (J_F^y - J_F^z)](2m_{1x}^2 - 1 + m_{1z}^2) = \\ & = (J_F^z - J_F^y)m_{1z}^2 + [(J_F^x - J_F^z) - (J_F^y - J_F^z)]m_{1x}^2 + const. \end{aligned} \quad (8)$$

This way the coefficient of the m_{1z}^2 term represents the uniaxial anisotropy; the (smaller) coefficient of the m_{1x}^2 term describes the remaining anisotropy around the z axis. Similar rearrangement can be made for m_2 and for all of the antiferromagnetic terms.

The total magnetization and the antiferromagnetic order parameter vectors are introduced as $\mathbf{m} = (\mathbf{m}_1 + \mathbf{m}_2)$ and $\mathbf{l} = (\mathbf{m}_1 - \mathbf{m}_2)$. Notice that $|\mathbf{m}| = 1$ corresponds to the saturation magnetization, and $|\mathbf{l}| = 1$ describes perfect antiferromagnetic order. In terms of these new parameters the Hamiltonian can be re-written as:

$$\begin{aligned} \mathcal{H}_{MF} = & 3NS^2 [J_{AF}^z(\mathbf{m}^2 - \mathbf{l}^2) + (J_{AF}^z - J_{AF}^y)(m_z^2 - l_z^2) + (J_{AF}^x - J_{AF}^z) - (J_{AF}^y - J_{AF}^z)(m_x^2 - l_x^2) \\ & + (J_F^z - J_F^y)(m_z^2 + l_z^2) + [(J_F^x - J_F^z) - (J_F^y - J_F^z)](m_x^2 + l_x^2)] + Ng\mu_B \mathbf{m} \mathbf{H} \end{aligned} \quad (9)$$

Here we re-grouped the terms in the antiferromagnetic coupling, emphasizing the anisotropy, without introducing new constraints. Neglecting fluctuations leads to $\mathbf{m}\mathbf{l} = 0$ and $\mathbf{m}^2 + \mathbf{l}^2 = 1$. Eliminating the \mathbf{l}^2 term finally yields:

$$\mathcal{H}_{MF}/N = \frac{A}{2} \mathbf{m}^2 + \frac{a}{2} m_z^2 + \frac{b}{2} l_z^2 + \frac{c}{2} m_x^2 + \frac{d}{2} l_x^2 - \mathbf{m} \mathbf{h} \quad (10)$$

where $A = 12S^2 J_{AF}^z$, $\mathbf{h} = g\mu_B \mathbf{S} \mathbf{H}$, and the anisotropy constants are expressed as

$$\begin{aligned} a = & 6S^2 (J_F^z - J_F^y + J_{AF}^z - J_{AF}^y), & b = & 6S^2 (J_F^z - J_F^y - J_{AF}^z + J_{AF}^y), \\ c = & 6S^2 [(J_F^x - J_F^z) - (J_F^y - J_F^z) + (J_{AF}^x - J_{AF}^z) - (J_{AF}^y - J_{AF}^z)] \\ d = & 6S^2 [(J_F^x - J_F^z) - (J_F^y - J_F^z) - (J_{AF}^x - J_{AF}^z) + (J_{AF}^y - J_{AF}^z)], \end{aligned} \quad (11)$$

Notice that Eq. 10 is applicable in the most general case, but the coupling constants reflect an expected hierarchy. A simple isotropic antiferromagnet is obtained for $a = b = c = d = 0$. For uniaxial anisotropy $c = d = 0$; the coefficients a and b describe anisotropies in the total magnetization and antiferromagnetic order, respectively. In our case coefficients c and d will be small.

VIII. APPENDIX B: SPIN RESONANCE FREQUENCIES.

For any given field direction there are two modes, denoted by ω_1 and ω_2 . At high external fields one can ne-

glect the small anisotropy within the easy plane, and take

$c = d = 0$. The frequencies were determined by Turov [14]. There are two principal frequencies for each mode, corresponding to external field applied parallel and perpendicular to the hard axis. The results are expressed in terms of effective fields:

$$\begin{aligned}
H_E &= A/M_0 \\
H'_E &= (A + a)/M_0 \\
H''_E &= (A - b)/M_0 \\
H_a &= a/M_0 \\
H_b &= b/M_0 \\
H_{EA} &= \sqrt{H_E H_b} \\
H_{\parallel} &= \sqrt{H''_E H_b} \\
H_{\perp} &= H_{\parallel} \frac{H'_E}{H''_E}
\end{aligned} \tag{12}$$

where M_0 is the saturation magnetization.

For field perpendicular to the hard axis one gets:

$$\begin{aligned}
\omega_1^{\perp} &= \gamma H \sqrt{1 + H_a/H_E} \quad \text{if } H < H_E \\
\omega_1^{\perp} &= \gamma \sqrt{H(H + H_a)} \quad \text{if } H > H_E \\
\text{and} \\
\omega_2^{\perp} &= \gamma H_{EA} \sqrt{1 - H^2/H_E^2} \quad \text{if } H < H_E \\
\omega_2^{\perp} &= \gamma \sqrt{(H - H''_E)(H - H_E)} \quad \text{if } H > H_E
\end{aligned} \tag{13}$$

where $\gamma = g\mu_B/\hbar$ in terms of the Bohr magneton and the g -factor. H_E is the saturation field; for $H > H_E$ all spins line up with the external field.

For the field direction parallel to the hard axis the saturation field is $H'_E > H_E$, since both the exchange coupling and the anisotropy work against the external field. The frequencies are:

$$\begin{aligned}
\omega_1^{\parallel} &= 0 \quad \text{if } H < H'_E \\
\omega_1^{\parallel} &= \gamma(H - H'_E) \quad \text{if } H > H'_E \\
\text{and} \\
\omega_2^{\parallel} &= \gamma H_{EA} \sqrt{1 + H^2/H_E^2} \quad \text{if } H < H'_E \\
\omega_2^{\parallel} &= \gamma(H - H_a) \quad \text{if } H > H'_E
\end{aligned} \tag{14}$$

The modes are shown in the high field part of Fig. 2. The ω_2^{\perp} mode reaches zero at the lower saturation field H_E . Below the saturation field the ω_1^{\perp} mode looks like a "free" spin resonance, except for the apparent g -factor is increased by a factor of $\sqrt{1 + H_a/H_E}$. Well above the saturation field the line is shifted to higher frequencies by the amount of $\gamma H_a/2$, but its slope is still γ . For fields parallel to the hard axis the ω_1^{\parallel} mode is zero at the upper saturation field. With the particular choice of parameters indicated in the Figure. The ω_2^{\parallel} mode is nearly independent of the field up to H'_E .

At low fields the anisotropy within the easy plane becomes important. A finite value of the parameter c (or d) has two important consequences. First, in zero field, the ω_1 mode (the "Goldstone mode") will shift to finite frequency. Second, the field dependence of the ω_1^{\perp} mode will be different for external fields applied in different directions within the easy plane. Instead of the two principal directions relative to the hard axis z (parallel and perpendicular), we will have to deal with three axes. We will identify these directions as the hard axis (parallel to z), the intermediate axis and the easy axis (formerly the two equivalent directions perpendicular to z).

For an approximate treatment of the $c \neq 0$ case we will turn to an early paper by Nagamiya [13], assuming $H \ll H_E$.

In finite fields along the hard axis the ω_1 mode is approximately independent of the field (this mode corresponds to the rotation of the spins in the easy plane, and it is excited with an oscillating magnetic field parallel to the static field). For fields in the intermediate direction the frequency of the mode increases; for the field applied in the easy direction there will be a spin-flop transition at $H = H'_{EA} = \sqrt{Ac}/M_0$.

$$\begin{aligned}
\omega_1^{hard} &= \gamma' H'_{EA} = \omega_1^{\parallel} \\
\omega_1^{int} &= \gamma' \sqrt{H^2 + H'^2_{EA}} \\
\omega_1^{easy} &= \gamma' \sqrt{\frac{\alpha}{2} + H^2 - \sqrt{\beta^2/4 + 2\alpha H^2}} \quad \text{if } H < H'_{EA} \\
\omega_1^{easy} &= \gamma' \sqrt{H^2 - H'^2_{EA}} \quad \text{if } H > H'_{EA}
\end{aligned} \tag{15}$$

Here we used $\alpha = H^2_{EA} + H'^2_{EA}$, $\beta = H^2_{EA} - H'^2_{EA}$. Nagamiya's calculation does not account for the increase of the apparent g -factor seen in Turov's low field result. Therefore we are using a modified $\gamma' = \gamma \sqrt{1 + H_a/H_E}$ here.

The anisotropy within the easy plane has no influence on the ω_2^{\parallel} mode (for fields parallel to the hard axis). For fields applied in the intermediate direction, the ω_2 mode is approximately independent of the field (except for a slight decrease in frequency, a precursor of the eventual saturation at H_E). When the field is in the easy direction, the spin-flop transition results in a jump of the ESR frequency.

$$\begin{aligned}
\omega_2^{hard} &= \gamma H_{EA} \\
\omega_2^{int} &= \gamma H_{EA} \\
\omega_2^{easy} &= \gamma \sqrt{\frac{\alpha}{2} + H^2 + \sqrt{\beta^2/4 + 2\alpha H^2}} \quad \text{if } H < H'_{EA} \\
\omega_2^{easy} &= \gamma \sqrt{H^2_{EA} - H'^2_{EA}} \quad \text{if } H > H'_{EA}
\end{aligned} \tag{16}$$

To ensure a seamless match to the high field calculation, in Fig. 4 we multiplied these frequencies with a saturation term, $\sqrt{1 - H^2/H_E^2}$. For the hard axis direction

we used the original ω_2^{\parallel} values. Neither this procedure, nor the modified γ' introduced earlier, can completely substitute for the full solution of the problem for arbitrary fields and parameters, but they are qualitatively correct.

trary fields and parameters, but they are qualitatively correct.

-
- [1] For a review, see M.F. Collins, O.A. Petrenko, *Can. J. Phys.* **75**, 605 (1997).
- [2] Y. Kitaoka, T. Kobayashi, A. Koda, H. Wakabayashi, Y. Niino, H. Yamakage, S. Taguchi, K. Amaya, K. Yamamura, M. Takano, A. Hirano, and R. Kanno, *J. Phys. Soc. Japan* **67**, 3703 (1998); F. Reynaud, D. Mertz, F. Celestini, J.M. Debierre, A.M. Ghorayeb, P. Simon, A. Stepanov, J. Voiron, C. Delmas, *Phys. Rev. Lett.* **86**, 3638 (2001); E. Chappel, M.D. Núñez-Regueiro, S. de Brion, G. Chouteau, V. Bianchi, D. Caurant, and N. Baffier, *Phys. Rev. B* **66**, 132412(2002).
- [3] M.D. Núñez-Regueiro, E. Chappel, G. Chouteau, and C. Delmas, *Eur. Phys. J. B* **16**, 37 (2000); M.V. Mostovoy and D.I. Khomskii, *Phys. Rev. Lett.* **89**, 227203 (2002); F. Vernay, K.Penc, P. Fazekas, F. Mila, *Phys. Rev. B* **70**, 014428 (2004); A.J. W. Reitsma, L. F. Feiner and A. M. Olés, *New Journal of Physics* **7**, 121 (2005).
- [4] E. Chappel, M.D. Núñez-Regueiro, G. Chouteau, O. Isnard and C. Darie, *Eur. Phys. J. B* **17**, 615 (2000).
- [5] E. Chappel, M.D. Núñez-Regueiro, F. Dupont, G. Chouteau, C. Darie, and A. Sulpice, *Eur. Phys. J. B* **17**, 609 (2000).
- [6] P.F. Bongers and U. Enz, *Solide State Com.* **4**, 153 (1966).
- [7] C. Darie, P. Bordet, S. de Brion, M. Holzapfel, O. Isnard, A. Lecchi, J.E. Lorenzo, and E. Suard, *Eur. Phys. J. B* **43**, 159 (2005).
- [8] M.J. Lewis, B.D. Gaulin, L. Filion, C. Kallin, A.J. Berlinsky, H.A. Dabkowska, Y. Qiu, J.R.D. Copley, *Phys. Rev. B*, **72**, 014408 (2005).
- [9] M. Holzapfel, S. de Brion, C. Darie, P. Bordet, E. Chappel, G. Chouteau, P. Strobel, A. Sulpice, M. D. Núñez-Regueiro, *Phys. Rev. B* **70**, 132410 (2004).
- [10] D. Talbayev, Ph.D. Thesis, Stony Brook, 2004
- [11] D. Talbayev, L. Mihaly, and J. Zhou, *Phys. Rev. Lett.* **93**, 017202 (2004); L. Mihaly, D. Talbayev, L.F. Kiss, J. Zhou, T. Feher, and A. Janossy, *Phys. Rev. B* **69**, 024414 (2004).
- [12] F. Keffer and C. Kittel, *Physical Review* **85**, 329 (1952).
- [13] T. Nagamiya, *Progr. Theor. Phys.* **11** 309 (1954).
- [14] E.A. Turov, "Physical Properties of Magnetically Ordered Crystals", Academic Press, New York, 1965.
- [15] S. de Brion et. al., to be published.
- [16] A.V.Chubukov and D.I. Golosov, *J. Phys.: Condens. Matter* **3**, 69 (1991).
- [17] L.E. Svistov, A.I. Smirnov, L.A. Prozorova, O.A. Petrenko, L.N.Demianets, A.Ya. Shapiro, *Phys. Rev. B* **67** 094434 (2003).
- [18] H. Tanaka, T. Ono, S. Maruyama, S. Teraoka, K. Nagata, H. Ohta, S. Okubo, S. Kimura, T. Kambe, H. Nojiri and M. Motokawa, *J. Phys Soc. Jpan.*, **72** Suppl. B, 84 (2003).